AD NUMBER

ADA182791

LIMITATION CHANGES

TO:

Approved for public release; distribution is unlimited.

FROM:

**Distribution authorized to U.S. Gov't. agencies and their contractors;
Administrative/Operational Use; MAY 1987. Other requests shall be referred to Office of Naval Research, 875 North Randolph Street, Arlington, VA 22203-1995.**

AUTHORITY

ONR ltr, dtd 6 Jul 1987

A METHOD FOR DYNAMIC FRACTURE INITIATION TESTING OF CERAMICS

J. Duffy, S. Suresh, K. Cho and E.R. Bopp

Division of Engineering
Brown University
Providence, Rhode Island 02912, USA

ONR-SDIO
Grant No. N00014-85-K-0687/2

National Science Foundation
Grant ENG-8451092

May, 1987

A METHOD FOR DYNAMIC FRACTURE INITIATION TESTING OF CERAMICS

by

J. Duffy[1], S. Suresh[2], K. Cho[3], and E.R. Bopp[4]

ABSTRACT

An experimental method is described whereby the dynamic fracture initiation toughness of ceramics and ceramic composites can be measured in pure tension or pure torsion at stress intensity factor rates of 10^5 to 10^6 MPa$\sqrt{m}$/s. In this procedure, circumferentially-notched cylindrical rods are subjected to uniaxial cyclic compression at room temperature to introduce a self-arresting, concentric Mode I fatigue pre-crack, following the technique presented by Suresh et al. (1987) and Suresh and Tschegg (1987). Subsequently, dynamic fracture initiation is effected by stress wave loading with a sharp-fronted pulse which subjects the specimen to a dynamic load inducing either Mode I or Mode III fracture. Instrumentation appropriate to the loading mode provides a record of average stress at the fracture site as a function of time. The capability of this method to yield highly reproducible dynamic fracture initiation toughness values for ceramics is demonstrated with the aid of experiments conducted on a polycrystalline aluminum oxide. The dynamic fracture toughness values are compared with the results obtained for quasi-static Mode I and Mode III fracture in the ceramic material at stress intensity factor rates of 10^{-1} to 1 MPa$\sqrt{m}$/s. Guidelines for the dynamic fracture initiation testing of ceramics and ceramic composites are discussed.

[1]Professor of Engineering, Fellow, ASME
[2]Associate Professor of Engineering, Member, ASME
[3]Post-Doctoral Fellow, Division of Engineering
[4]Undergraduate Research Assistant, Division of Engineering

INTRODUCTION

Ceramics and ceramic-matrix composites invariably contain flaws in the form of microcracks which may be induced during synthesis, fabrication or pre-stressing of the material. In engineering applications employing these brittle solids, design considerations are aimed at determining safe operating conditions to preclude the initiation of catastrophic fracture from pre-existing microscopic flaws. In the past, the static or quasi-static fracture initiation behavior of ceramics has been the subject of considerable research. However, whether by design or otherwise, in many practical situations ceramic components may be subjected to dynamic loading conditions, as for example, in armor plate. It is, therefore, of paramount importance to understand the dynamic fracture initiation characteristics of these brittle solids. Despite the clear need, dynamic fracture behavior of ceramics has remained a relatively unexplored area of research.

The most commonly employed dynamic fracture test is the Charpy impact test, because of its relatively low cost and the ease with which it is performed. While Charpy tests provide important information about the fracture energy and are useful for material screening purposes, the interpretation of the results in terms of fracture mechanics concepts is not unambiguous, as was shown by Kobayashi et al. (1986). In the Charpy test, plane strain conditions are not achieved and the energy value obtained encompasses the entire fracture process which includes both fracture initiation and growth until catastrophic separation. Consequently, *non-conservative* estimates of the critical fracture parameters may be derived from such an experiment. The results of experiments with specimens not containing a fatigue crack are likely to be a strong function of the artifacts of the experimental conditions, namely the specimen geometry and the notch geometry. To our knowledge, no results are currently available in the literature on critical stress intensity factors for dynamic fracture initiation in ceramics.

The determination of dynamic fracture properties for brittle solids is a task which is subject to considerable experimental difficulties because of the problems associated with pre-cracking the specimen prior to the fracture test. Unlike ductile metallic materials, brittle ceramics, in general, do not exhibit any stable fatigue crack growth under tensile cyclic loads applied at room temperature. This imposes stringent restrictions in obtaining "valid" estimates of critical stress intensity factors for fracture initiation under quasi-static or dynamic loading conditions. In the past, attempts have been made to circumvent this problem by resorting to fracture test methods, such as the

indentation technique (e.g. Lawn and Wilshaw, 1975), or the chevron-notched short rod/bar method (Barker, 1977), where the loading conditions, specimen geometry and the crack geometry are designed to force a certain amount of stable crack growth. It is now well-established that the results derived from such methods may be subject to some variation and error because of the uncertainties in determining the crack shape and the critical stress intensity factor (see, for example, Suresh et al., 1987). An ideal solution to this problem is the development of methods capable of introducing a "sharp" through-thickness fatigue crack (in a plate) or a concentric flaw (in a cylindrical rod) in brittle ceramics prior to the fracture test, as is customary in the case of metallic materials. Such controlled pre-cracks are essential for the unequivocal characterization of fracture behavior using linear elastic fracture mechanics and for obtaining "valid" and reproducible estimates of the critical fracture parameters. This also enables the direct extrapolation of the well-established test methods currently available for metals to the static and dynamic fracture testing of brittle ceramics.

Recently, Ewart and Suresh (1986, 1987) demonstrated that the application of cyclic compressive stresses to notched plates of ceramics and ceramic composites leads to stable fatigue crack growth even at room temperature, Figure 1. The through-thickness fatigue cracks propagate at a progressively decelerating velocity along the plane of the notch, in a direction macroscopically perpendicular to the compression axis. The principal driving force for this Mode I fatigue phenomenon is now considered to be the generation of residual tensile stresses at the root of the notch upon unloading from the maximum far-field compressive stress (Brockenbrough and Suresh, 1987). Detailed finite element calculations have shown that residual tensile stresses are induced at the notch-tip when permanent strains are retained in the near-tip region under far-field cyclic compression, irrespective of whether the deformation mechanism is dislocation plasticity, microcracking, phase transformation or creep (Brockenbrough and Suresh, 1987). Consequently, a macroscopically similar Mode I fracture behavior is observed under far-field cyclic compression in a wide range of materials spanning the very ductile metals to extremely brittle solids, despite vast differences in their microscopic modes of deformation and failure. As the local zone of residual tension, which is responsible for Mode I fatigue crack growth, is embedded in material elastically strained in compression, crack advance under far-field cyclic compression is intrinsically stable even in brittle solids. Recent work has shown that the phenomenon of stable fatigue crack growth under far-field cyclic compression offers a unique capability for pre-cracking ceramic fracture test specimens (Suresh and Tschegg, 1987).

In this paper, we present experimental methods for determining the dynamic fracture initiation properties, of ceramics subjected either to pure tension or pure torsion. Circumferentially notched cylindrical rods of a polycrystalline aluminum oxide were pre-cracked in uniaxial cyclic compression to introduce a concentric Mode I fatigue pre-crack. Subsequently the specimens were subjected to dynamic loads either in Mode I or in Mode III. Dynamic fracture initiation is effected in either case by stress wave loading of the fracture site by means of a sharp-fronted pulse, as first described by Duffy et al. (1971) and by Costin et al. (1976). For Mode I fracture a tensile pulse is propagated along the bar, whereas for Mode III fracture a torsional pulse is employed. Instrumentation appropriate for the loading mode provides a record of average stress at the fracture site as a function of time. Based on the experimental data, the critical value of the crack-tip stress intensity factor, K_{Ic} or K_{IIIc}, is evaluated at a loading rate of the order of 10^6 MPa$\sqrt{m}$/s or 10^5 MPa$\sqrt{m}$/s, respectively. These loading rates are equal to or perhaps slightly greater than can be achieved in the Charpy test and lie beyond the range obtainable by means of programmable testing machines. While testing machines can load rapidly, they cannot be employed in the stress wave regime since wave reflections would occur at the many interfaces in the load column, leading to incorrect values of load and displacement.

The dynamic Mode I and Mode III fracture initiation properties of the ceramic are shown to be greater than corresponding values obtained under quasi-static loading conditions ($K_{I,III} \simeq 10^{-1}$ - 1 MPa$\sqrt{m}$/s). The fracture surface morphology is examined both optically and in the scanning electron microscope in an attempt to rationalize the apparent differences in the measured fracture toughness in response to the changes in loading mode.

EXPERIMENTAL TECHNIQUE

Pre-Cracking Method

Figure 2 is a schematic diagram showing the geometry of the dynamic fracture test specimens. The specimen dimensions are: d_o = 19mm, d_i = 9mm, L = 58 mm, L_1 = 28 mm, t = 1.8 mm, $\theta = 60^\circ$ and ρ = 0.127 mm. The notch was introduced using a diamond wheel. The specimen was pre-cracked under fully compressive cyclic stresses ranging from about -50 MPa to -785 MPa at a constant frequency of about 15 Hz (sinusoidal waveform) in the laboratory environment (temperature $\simeq 23^\circ$C and relative

humidity $\simeq$ 40%). The presence of a uniform, concentric fatigue pre-crack at the root of the notch was verified *a posteriori* through optical and scanning electron microscopy observations made after fracturing the test specimen. The notch geometry and compression fatigue loads were selected such that the length of the fatigue crack (between 65 and 150 μm) was substantially greater than any characteristic microstructural dimension (grain size = 3 μm), but short enough to minimize fracture surface abrasion in the torsion experiments.

Dynamic Testing in Tension

Figure 3 shows the experimental arrangement employed for the Mode I dynamic fracture test. The ceramic specimen, shown in Figure 2a, is held between two long steel bars each 2.54 cm in diameter. To grip the specimen securely, it is inserted within two axial holes machined into the ends of the bars and held in place by a cemented joint. Precise machining and a fine air vent are used to avoid any gap between the end of the ceramic specimen and the steel bar. As shown in Figure 3, a tensile loading pulse is initiated at one end of the apparatus by the detonation of an explosive charge placed against a loading head suitably shaped so that the initial pulse propagating down the bar is one of tension. Fracture is obtained when this tensile pulse loads the fatigue crack in the ceramic specimen.

An experimental arrangement quite similar to the present one has been in use for some time to study dynamic fracture initiation in steel specimens (Costin and Duffy, 1979; Duffy et al., 1985) and more recently in a metal-matrix composite (Marchand et al., 1986). There is, however, one essential difference between the past experiments and the present one. In the past the entire bar, including loading ends and the notched section, was machined from a single metal rod 2.54 cm in diameter. In the present tests, the ceramic specimen is inserted between the two loading bars.

Accurate data reduction with this arrangement requires that there be no impendance change along the length of either of the loading bars. In the present instance, the impendance of axial waves in the aluminum oxide ceramic happens to match closely that of the steel. It may be shown that for an axial wave propagating along a slender cylindrical elastic rod the impendance is given by ρcA, where ρ is the material's density, c the wave velocity and A the cross-sectional area of the rod. In the present test

$$(\rho cA)_{ceramic} \doteq (\rho cA)_{steel} \tag{1}$$

The specific gravity of steel may be taken as 7.85 while the wave velocity in a cylindrical elastic rod of steel is about 5,050 m/s. The ceramic is considerably stiffer but much lighter, its specific gravity is about 3.9 and the wave velocity 9,500 m/s. A simple calculation shows that the difference between the two impedances is less than 5%, and thus could be compensated for by a change in diameter of about 2%. Obviously, as a result of the method of gripping the specimen, Figure 4, some wave reflections will occur within the steel surrounding the ceramic. Their effect must be insignificant since in the present experiments no reflected disturbance is observed preceding the main pulse indicating that the impedance mismatch is too small to be detected on the observed scale. Thus the transmitted pulse, which is monitored by axial gages mounted on the transmitter bar, gives an accurate measure of the axial load transmitted through the fatigue section of the ceramic specimen. A typical transmitted pulse is shown in Figure 4. The peak in the curve provides the maximum transmitted load which, for a brittle material, represents the critical load at fracture initiation. This critical load is used to calculate the critical value of the crack-tip stress intensity factor through (Tada, Paris, and Irwin, 1973)

$$K_I = \frac{2P}{\pi d_i^2} \left\{ \frac{\pi d_i}{2} (1 - \underline{d}) \right\}^{1/2} \left\{ 1 + 0.5\underline{d} + 0.375\underline{d}^2 - 0.363\underline{d}^3 + 0.731\underline{d}^4 \right\} \qquad (2)$$

where P is the applied load at fracture initiation, $\underline{d} = d_i/d_o$, and d_i and d_o are defined in Figure 2. Note that in applications involving an impedance mismatch, the cross sectional areas for the specimen and the loading bars can be chosen appropriately to satisfy Equation (1).

Dynamic Testing in Torsion

The arrangement for Mode III fracture follows along the same principles. The torsional loading apparatus shown in Figure 5 is used to provide a sharp-fronted torsional loading pulse. In this instance, the specimen is machined with short hexagonal flanges, Figure 2b. These flanges enter matching hexagonal holes at the ends of the loading bars. To prevent any relative motion between the bars and the flanges, each flange is held in place by twelve small set-screws.

This apparatus has been employed successfully in the past to study the dynamic stress-strain behavior of metals (Duffy, 1979). The torsional loading pulse can be initiated through explosive loading but, in the present tests, a stored torque is used

(Senseney et al., 1978). This torque is stored at the left end of the bar between the torque pulley and the clamp. To obtain a sharp-front stress pulse, rapid release of the clamp is essential and this is effected by the fracture of a brittle breaker piece. By this method loading rates on the order of 10^5 MPa$\sqrt{m}$/s are achieved. The transmitted pulse is recorded by strain gages mounted at 45° to the axis of the bar. As in the case of Mode I fracture, the peak in this curve provides the maximum value of the transmitted torque, which represents the critical torque at fracture.

The critical stress intensity factor for Mode III fracture is determined from (Tada, Paris, and Irwin, 1973).

$$K_{III} = \frac{6T}{\pi d_i^3} \left\{\frac{\pi d_i}{2} (1 - \underline{d})\right\}^{1/2} \left\{1 + 0.5\underline{d} + 0.375\underline{d}^2 + 0.3125\underline{d}^3 + 0.273\underline{d}^4 + 0.208\underline{d}^5\right\} \quad (3)$$

where T is the applied torque at the instant of fracture initiation.

The dynamic fracture behavior of the ceramic material is compared and contrasted with the results obtained under quasi-static loading conditions, i.e. at stress intensity rates of about 0.1 - 1.0 MPa$\sqrt{m}$/s. The specimen geometry and pre-cracking procedure for the quasi-static tests were similar to those employed in the dynamic experiments. After introducing the fatigue pre-crack, the quasi-static test specimen was fractured in pure tension using a specially-designed friction grip (consisting of a slotted tube tightened by a collet) which was connected to the load train of the electro-servohydraulic test machine through universal joints. The details of the quasi-static tension and torsion tests can be found in the paper by Suresh and Tschegg (1987).

Test Material

The material investigated in this work was a 99.8% pure polycrystalline aluminum oxide, commercially available as Grade AD998 from Coors Porcelain Co., Golden, Colorado. The impurities and grain boundary phases in this material consist of SiO_2, MgO, Ca, Na and Fe. The average grain size is about 3μm and the grain size range is typically 1-6 μm. The room temperature properties of this material, as reported by the supplier, are: Young's modulus = 345 GPa, flexure strength = 330 MPa, unconstrained compressive strength = 2071 MPa and specific gravity = 3.9.

RESULTS AND DISCUSSION

Mode I Fracture

Figure 6a is an optical micrograph of the fracture surface of AD998 alumina quasi-statically fractured in pure tension. The concentric fatigue crack (visible as the light region at the tip of the circumferential notch) was propagated under far-field cyclic compression to a depth of about 40 μm. The critical stress intensity for quasi-static Mode I fracture initiation, K_{Ic}, was found to be 3.35 MPa$\sqrt{m}$ ± 0.05 MPa$\sqrt{m}$ from several experiments conducted at $\dot{K}_I \simeq 0.1$ MPa$\sqrt{m}$/s. The flatness of the fracture surface provides an indication of the purely tensile failure mode in these experiments. Furthermore, the alignment of the load train was checked by mounting 3 strain gages (120° apart) along the circumference of the ceramic rod, indicating that the differences in the strain gage output was less than 1%.

Figure 6b is a scanning electron micrograph of the quasi-static Mode I fracture specimen showing the boundary between the fatigue pre-crack and quasi-static tensile fracture. This fractograph reveals a predominantly intergranular mode of separation during both fatigue and quasi-static fracture. (The presence of debris particles of Al_2O_3 formed during high frequency contact between fracture surfaces can be noticed in the compression fatigue region).

The appearance of the fracture surfaces of dynamic tensile specimens is shown in Figure 7 at different magnifications. The depth of the fatigue crack in these experiments was typically about 70 μm. The critical stress intensity factor for dynamic fracture initiation was 5.62 ± 0.50 MPa$\sqrt{m}$ (from four experiments summarized in Table I) at a loading rate, $\dot{K}_I \simeq 10^6$ MPa$\sqrt{m}$/s. As can be seen from Figure 7a, the fracture surface is predominantly flat with the exception of a small region in the center of the specimen. This small rougher region may be due to the fact that the stress field during passage of the loading pulse is not fully symmetric to either side of the fracture plane. As indicated in the analysis of Nakamura et al. (1985), the loading pulse creates a near-tip stress field that is symmetric, but far from the crack tip the stress field is unsymmetric. Fortunately, the value of K_I is based on data obtained at fracture initiation, i.e. depends principally on the near-tip field. However, the far field may well influence the appearance of the subsequent fracture surface.

The dynamic fracture initiation toughness of the fine-grained alumina is about 50% higher than that measured under quasi-static loading rates. An examination of the microscopic fracture modes in the scanning electron microscope reveals that the initiation of fracture occurs by a predominantly intergranular failure mode irrespective of whether the loading is quasi-static or dynamic (Figures 6b and 7b). However, under dynamic conditions, there is evidence of a relatively greater percentage of transgranular failure. The fraction of the fracture surface, within 200 μm of the quasi-static fracture initiation region, where transgranular failure occurred was measured to be up to 34% (with a median 25%) using a computerized image analysis system. The corresponding maximum value of transgranular fracture under quasi-static tensile loads was only about 17%. The origin of such differences in microscopic separation modes cannot be pinpointed from the present set of experiments. However, this observation may provide one possible rationale for the lower fracture toughness in the quasi-static test where the intergranular separation leads to a lower fracture energy (e.g., Rice et al., 1981). Other factors that may play a role in promoting this stress rate dependence of toughness include the effects of loading rate on microcrack nucleation and on frictional sliding resistance of the surfaces of the microcrack.

Mode III Fracture

In distinct contrast with the macroscopically flat fracture surfaces observed under tensile loading, a highly tortuous and rough fracture surface was observed under torsional loads in both the quasi-static and dynamic tests. Figure 8 shows the appearance of a Mode III fracture surface obtained in the compression fatigue pre-cracked rod of alumina at quasi-static loading rates. The frictional resistance to shear along the notch plane leads to crack deviation which is reflected in the tortuous fracture path. A commonly observed direction of fracture under far-field torsion in cylindrical rods is along the planes at 45° to the longitudinal axis where the principal tensile stresses induce a local Mode I separation. Due to such multiple crack deflection and the consequent fracture surface interference, the apparent Mode III fracture initiation toughness at quasi-static rates is found to be 7.63 ± 0.2 MPa$\sqrt{m}$ (Table I). Recent work by Suresh and Tschegg (1987) on combined Mode I - Mode III fracture of alumina at quasi-static rates has shown that the apparent fracture initiation toughness increases monotonically with the introduction of torsional loads. The combined influence of crack path tortuosity and crack face

interference under torsion leads to an increase in the apparent fracture initiation toughness by a factor of about 2.3 as the loading mode is changed from pure tension to pure torsion.

The scanning electron micrographs of the fracture surfaces obtained for specimens quasi-statically loaded in torsion are given in Figure 9 at different magnifications. An interesting feature of the microscopic failure mode is evidence of flat transgranular shear facets induced in torsional loading, although the principal failure mode is intergranular separation in torsion. Such transgranular "sheets" arising from abrasion span tens of grains (e.g. Figure 9b) where the surface features are unchanged across grain boundaries. In contrast with this, the transgranular cleavage steps observed under quasi-static and dynamic tension generally exhibit a change in orientation of the cleavage facets across grain boundaries.

The dynamic fracture initiation toughness in Mode III was 10.24 ± 0.50 MPa$\sqrt{m}$ using the torsional Kolsky (split-Hopkinson) bar method at $\dot{K}_{III} \simeq 10^5$ MPa$\sqrt{m}$/s. The overall mode of failure in dynamic torsion was similar to that observed under quasi-static torsion (Figure 10). However, there appears to be an enhancement in fracture surface roughness and extent of transgranular failure under dynamic loading conditions (e.g. Figure 10b). For the dynamic torsion tests, the fatigue pre-crack lengths shown in Table I are higher than the corresponding values for the other cases. Our parallel studies (Suresh and Tschegg, 1987) have shown that for the range of pre-crack lengths obtained in this work, the differences in fracture surface abrasion during torsion are not large enough to cause any significant differences in the measured Mode III fracture initiation toughness.

The present results indicate that the use of quasi-static fracture initiation toughness values for failure under dynamic loading of ceramics is likely to yield a *conservative* design criterion. Our experiments for both quasi-static and dynamic fracture of alumina, in conjunction with the parallel study by Suresh and Tschegg (1987), also indicate that apparent Mode III fracture toughness (as well as fracture toughness under combined Mode I - Mode III) is always greater than the Mode I toughness. We note here that attempts have been made to measure the torsional fracture of ductile solids (e.g. steels) with a superimposed tensile load which would minimize (or even eliminate) crack face interference by inducing a crack opening displacement larger than the average asperity height. However, such an approach does not appear feasible for ceramics where the maximum crack opening displacement is always smaller than the average height of the fracture surface asperities even if the

superimposed tension is great enough such that $K_I \rightarrow K_{Ic}$. This implies that the fracture initiation properties of ceramics under torsional loading conditions are always likely to be influenced by the abrasion between the crack faces. (Note, however, that the direct measurement of fracture initiation toughness in notched rods of ceramics containing no fatigue pre-cracks cannot be construed as valid, because the geometry of the notch-tip strongly influences the near tip stress field and hence the apparent toughness). A detailed description of the effects of fracture surface tortuosity and abrasion on the apparent enhancement in fracture toughness of ceramics under torsional loads can be found in the work of Suresh and Tschegg (1987).

Although the experiments reported in this paper pertain to a (nominally) single phase, polycrystalline $A\ell_2O_3$ ceramic material, we note that the method proposed here is equally applicable to the dynamic fracture initiation testing of ceramic-matrix or metal-matrix composites reinforced by ceramic particulates or whiskers, transformation-toughened ceramics and cemented carbides. Recent work by Ewart and Suresh (1987) has shown that controlled fatigue pre-cracks can be introduced under far-field cyclic compression in multi-phase brittle solids (e.g., Y_2O_3 - partially stabilized zirconia and WC-Co) and their composites (Si_3N_4 or $A\ell_2O_3$ matrix with SiC whiskers). It should, however, be noted that attempts to initiate a Mode I fatigue pre-crack in single crystals of alumina and in soda-lime glass under compression fatigue have thus far proved unsuccessful (Ewart and Suresh, 1987).

4. Conclusions

1. An experimental procedure is described whereby the fracture initiation toughness of brittle ceramics and ceramic composites can be determined at stress intensity factor rates of 10^5 to 10^6 MPa$\sqrt{m}$ under pure tension or pure torsion loading conditions. The critical stress intensity factor for dynamic fracture initiation is obtained in Mode I or Mode III by stress wave loading of circumferentially notched cylindrical rods of ceramic materials which are fatigue pre-cracked in uniaxial cyclic compression.

2. Experimental results obtained for a fine grained aluminum oxide reveal that the Mode I and Mode III dynamic fracture initiation toughness values ($\dot{K}_I$, $\dot{K}_{III}$ = 10^5 - 10^6 MPa$\sqrt{m}$/s) are about 50% higher than the corresponding quasi-static toughness ($\dot{K}_I$, $\dot{K}_{III} \simeq$ 0.1 MPa$\sqrt{m}$/s).

3. For both the quasi-static and dynamic loading modes, the stress intensity factor for fracture initiation is significantly higher in Mode III than in Mode I.

4. The test methods described yield highly reproducible fracture toughness values in either mode of fracture.

5. Acknowledgements

The research support of the Office of Naval Research, Structural Mechanics Program under ONR-SDIO grant N00014-85-K-0687 and of National Science Foundation grant NSF-ENG-8451092 are gratefully acknowledged. Thanks are due also to Mr. George LaBonte for his help in carrying out the experiments.

REFERENCES

Barker, L.M. (1977), "A Simplified Method for Measuring Plane Strain Fracture Toughness," *Engineering Fracture Mechanics*, Vol. 9, No. 2, pp. 361-370.

Brockenbrough, J.R. and Suresh, S. (1987) "Constitutive Behavior of a Microcracking Brittle Solid in Cyclic Compression," *J. Mech. Physics Solids*, Vol. 35, in press.

Costin, L.S., Duffy, J. and Freund, L.B. (1976) "Fracture Initiation in Metals Under Stress Wave Loading Conditions," Fast Fracture and Crack Arrest, *ASTM*, STP 627, pp. 301-318.

Costin, L.S. and Duffy, J., (1979) "The Effect of Loading Rate and Temperature on the Initiation of Fracture in a Mild, Rate-Sensitive Steel," *J. Eng. Mat. Tech.*, pp. 258-264.

Duffy, J., Campbell, J.D. and Hawley, R.H., (1971) "On the Use of a Torsional Split Hopkinson Bar to Study Rate Effects in 1100-0 Aluminum," *J. Appl. Mech.*, March, pp. 83-91.

Duffy, J., Shih, C.F., Freund, L.B. and Hawley, R.H. (1985) "Fracture Initiation by Stress Wave Loading," Proc. Int'l. Conf. Mech. and Phys. Behavior of Mat. under Dynamic Loading, *J. de Physique* Vol. 46, Coll. C5, pp. 163-169.

Duffy, J., (1979), "The J.D. Campbell Memorial Lecture: Testing Techniques and Material Behaviour at High Rates of Strain," Proc. Second Conf. Mech. Properties of Mat. at High Rates of Strain, Ed: J. Harding, Oxford, England, pp. 1-15.

Ewart, L. and Suresh, S. (1986) "Dynamic Fatigue Crack Growth in Polycrystalline Alumina under Cyclic compression," *J. Mat. Science Letters*, Vol. 5, No. 8, pp. 774-778.

Ewart, L. and Suresh, S. (1987) "Crack Propagation in Ceramics under Cyclic Loads," *J. Materials Science*, Vol. 22, No. 4, pp. 1173-1192.

Lawn, B.R. and Wilshaw, T.R. (1975), "Review: Indentation Fracture: Principles and Applications," *J. Mat. Science*, Vol. 10, No. 4, pp. 1049-1081.

Kobayashi, T., Niinomi, M., Koide, Y. and Matsunuma, K. (1986), "Instrumented Impact Testing of Ceramics," Proc. 2nd Conf. of Asian-Pacific Congress on Strength Evaluation, Seoul, Korea, in press.

Marchand, A. Duffy, J., Christman, T.A. and Suresh, S., (1986), "An Experimental Study of the Dynamic Mechanical Properties of an Al-SiC_w Composite," Brown University Report ONR/SDIO N00014-85-K-06871/1.

Nakamura, T., Shih, C.F. and Freund, L.B., (1985) "Elastic Plastic Analysis of a Dynamically Loaded Circumferentially Notched Round Bar," *Engineering Fracture Mechanics*, Vol. 22, No. 3, pp 437-452.

Rice, R.W., Freiman, S.W. and Becher, P.R., (1981), "Grain-Size Dependence of Fracture Energy in Ceramics: I, Experiment," *J. Amer. Ceramic Soc.*, Vol. 64, No. 6, pp. 345-350.

Senseny, P.E. Duffy, J. and Hawley, R.H., (1978), "Experiments on Strain Rate History and Temperature Effects During the Plastic Deformation of Close-Packed Metals," *J. of Applied Mech.*, pp. 60-66.

Suresh, S. and Tschegg, E.K. (1987) "Combined Mode I - Mode III Fracture of Fatigue Pre-Cracked Alumina," *J. Amer. Ceramic Soc.*, Vol. 70, in press.

Suresh, S., Ewart, L., Slaughter, W., Maden, M. and Nguyen, M. (1987) "Fracture Toughness Measurements in Ceramics: Pre-Cracking in Cyclic Compression," *J. Mat. Science*, Vol. 22, No. 4, pp 1271-1276.

Tada, H., Paris, P.C. and Irwin, G.R., (1973) "The Handbook of Stress Intensity Factors," Del Research Corp., Hellertown, PA.

FIGURE CAPTIONS

Figure 1 Examples of Mode I fatigue crack growth in single-edge notched specimens of ceramics and ceramic composites subjected to uniaxial cyclic compression at room temperature. Compression axis is vertical. (a) Polycrystalline Al_2O_3 (b) hot pressed Si_3N_4 (c) Al_2O_3 with 30 v/o SiC_w

Figure 2 Schematic diagram of the dynamic fracture test specimens for (a) Mode I (tensile) and (b) Mode III (torsional). The notch tip geometry is the same in the two specimens.

Figure 3 Schematic diagram of the experimental arrangement for the Mode I dynamic fracture test.

Figure 4 Photograph of an oscilloscope trace of a typical transmitted pulse in dynamic Mode I fracture.

Figure 5 Schematic diagram of the torsional Kolsky bar for dynamic Mode III fracture.

Figure 6 Photographs of the quasi-static Mode I fracture surface of polycrystalline Al_2O_3. (a) Optical micrograph (b) SEM fractograph showing the fatigue pre-crack and fracture initiation area.

Figure 7 Photographs of dynamic Mode I fracture surfaces of polycrystalline Al_2O_3. (a) Optical micrographs (b) SEM fractograph showing the fatigue pre-crack and fracture initiation area.

Figure 8 Optical micrograph of the quasi-static Mode III fracture surface of polycrystalline Al_2O_3.

Figure 9 SEM fractographs of a quasi-static Mode III fracture surface of polycrystalline Al_2O_3. (a) shows the fatigue pre-crack and fracture initiation area, and (b) shows the transgranular facets in the fracture initiation area.

Figure 10 Dynamic Mode III fracture surface of polycrystalline Al_2O_3. (a) Optical micrograph. (b) SEM fractograph showing the transgranular facets in the fracture initiation area.

TABLE

FRACTURE TEST RESULTS

(a) Mode I

	Test No.	Width of Fatigue Annulus (μm)	Max. Load (N)	K_{Id}, K_{Ic} (MPa$\sqrt{m}$)
Dynamic Tests	1	70	6015	5.64
	2	65	5390	5.06
	3	70	6000	5.63
	4	70	6540	6.13
Quasi-Static Tests	1	35	3660	3.39
	2	50	3585	3.34
	3	40	3545	3.29

(b) Mode III

	Test No.	Width of Fatigue Annulus (μm)	Max. Torque (Nm)	K_{IIId}, K_{IIIc} (MPa$\sqrt{m}$)
Dynamic Tests	1	150	31.8	10.78
	2	120	30.6	10.19
	3	140	30.1	10.14
	4	150	29.0	9.83
Quasi-Static Tests	1	35	23.5	7.46
	2	55	24.2	7.78
	3	40	23.9	7.61

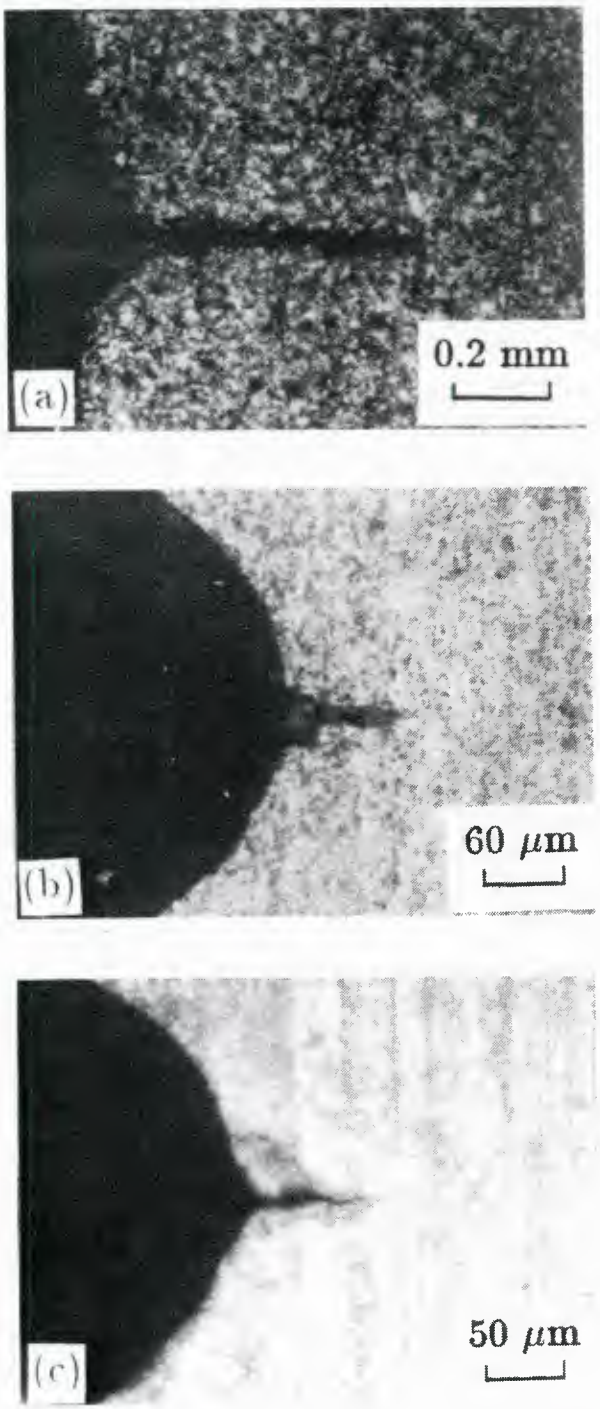

Figure 1 Examples of Mode I fatigue crack growth in single-edge notched specimens of ceramics and ceramic composites subjected to uniaxial cyclic compression at room temperature. Compression axis is vertical.
(a) Polycrystalline Al_2O_3 (b) hot pressed Si_3N_4 (c) Al_2O_3 with 30 v/o SiC_W

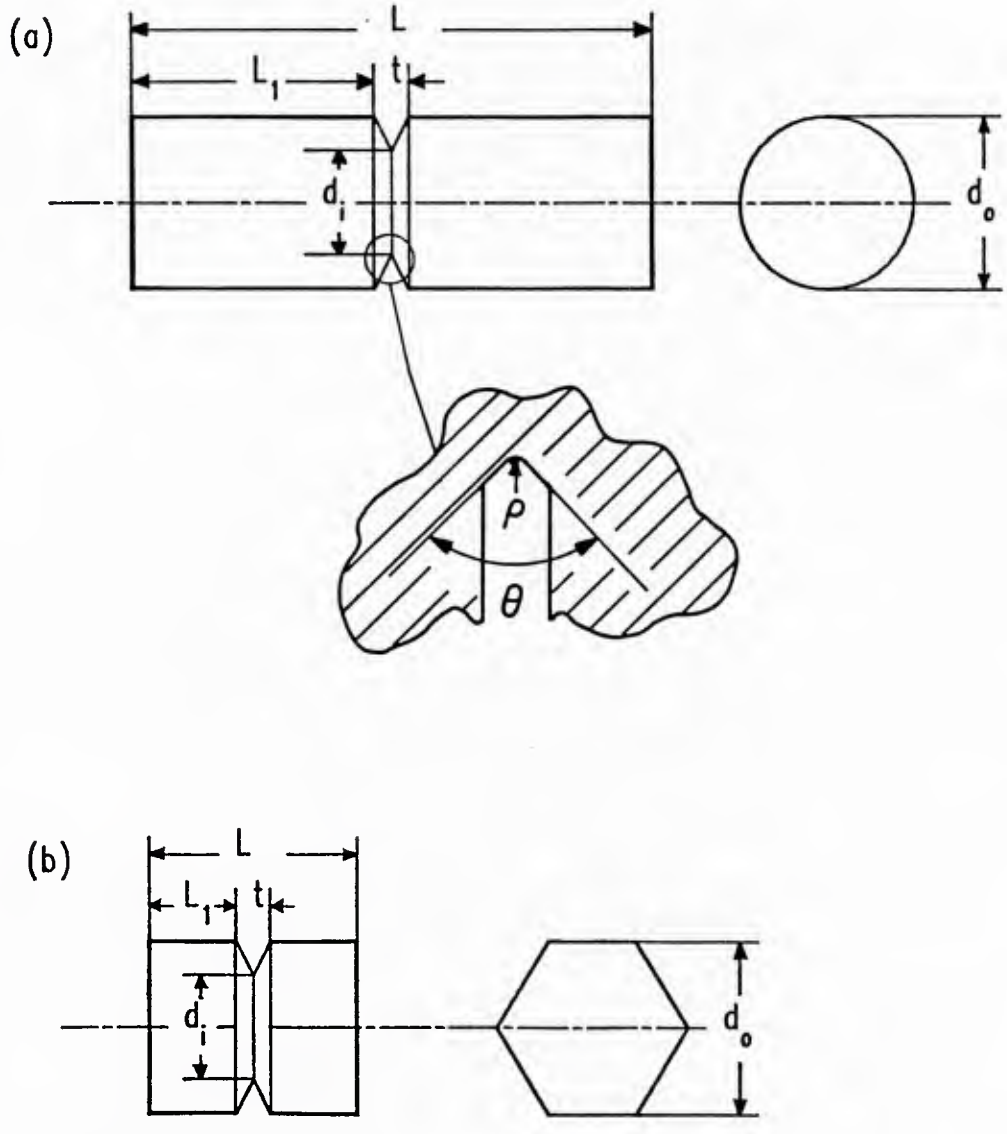

Figure 2 Schematic diagram of the dynamic fracture test specimens for (a) Mode I (tensile) and (b) Mode III (torsional). The notch tip geometry is the same in the two specimens.

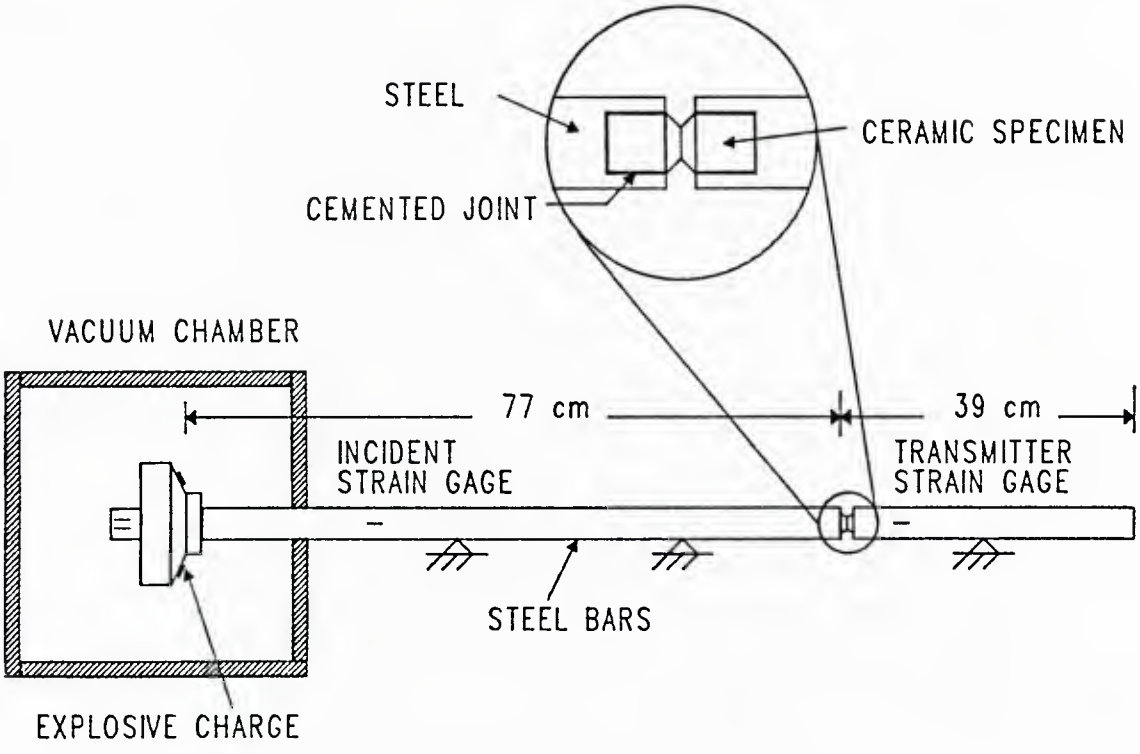

Figure 3 Schematic diagram of the experimental arrangement for the Mode I dynamic fracture test.

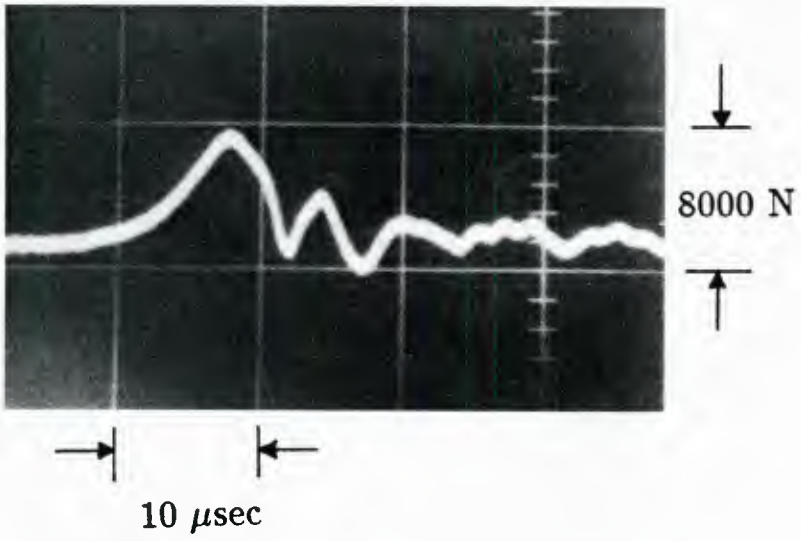

Figure 4 Photograph of an oscilloscope trace of a typical transmitted pulse in dynamic Mode I fracture.

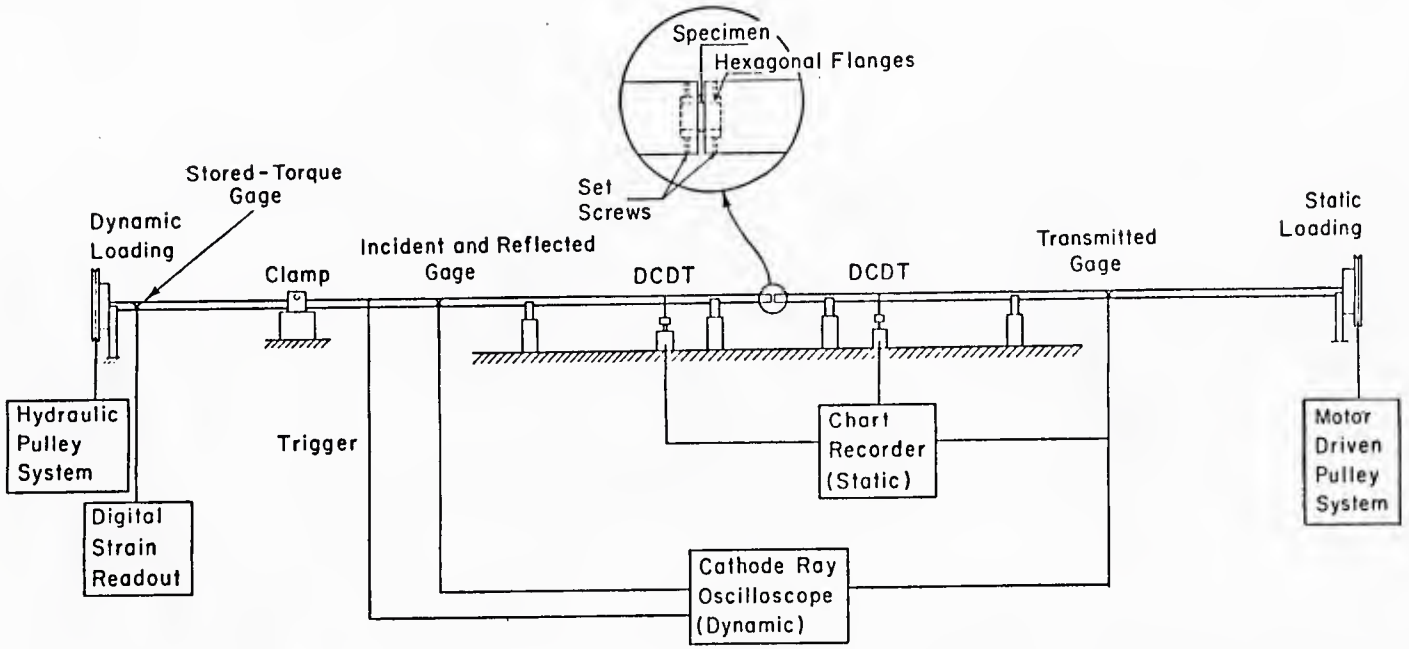

Figure 5 Schematic diagram of the torsional Kolsky bar for dynamic Mode III fracture.

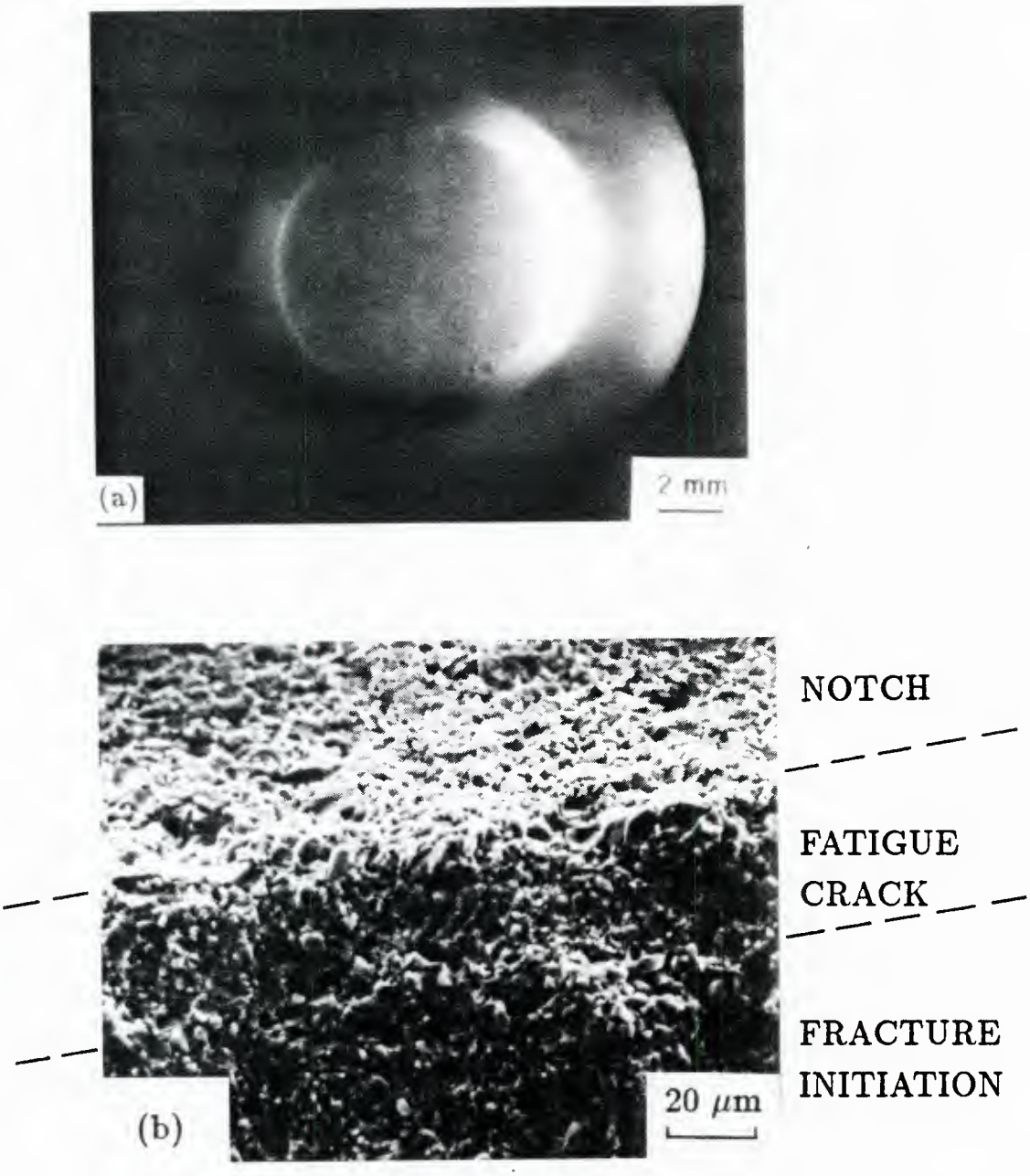

Figure 6 Photographs of the quasi-static Mode I fracture surface of polycrystalline Al_2O_3. (a) Optical micrograph (b) SEM fractograph showing the fatigue pre-crack and fracture initiation area.

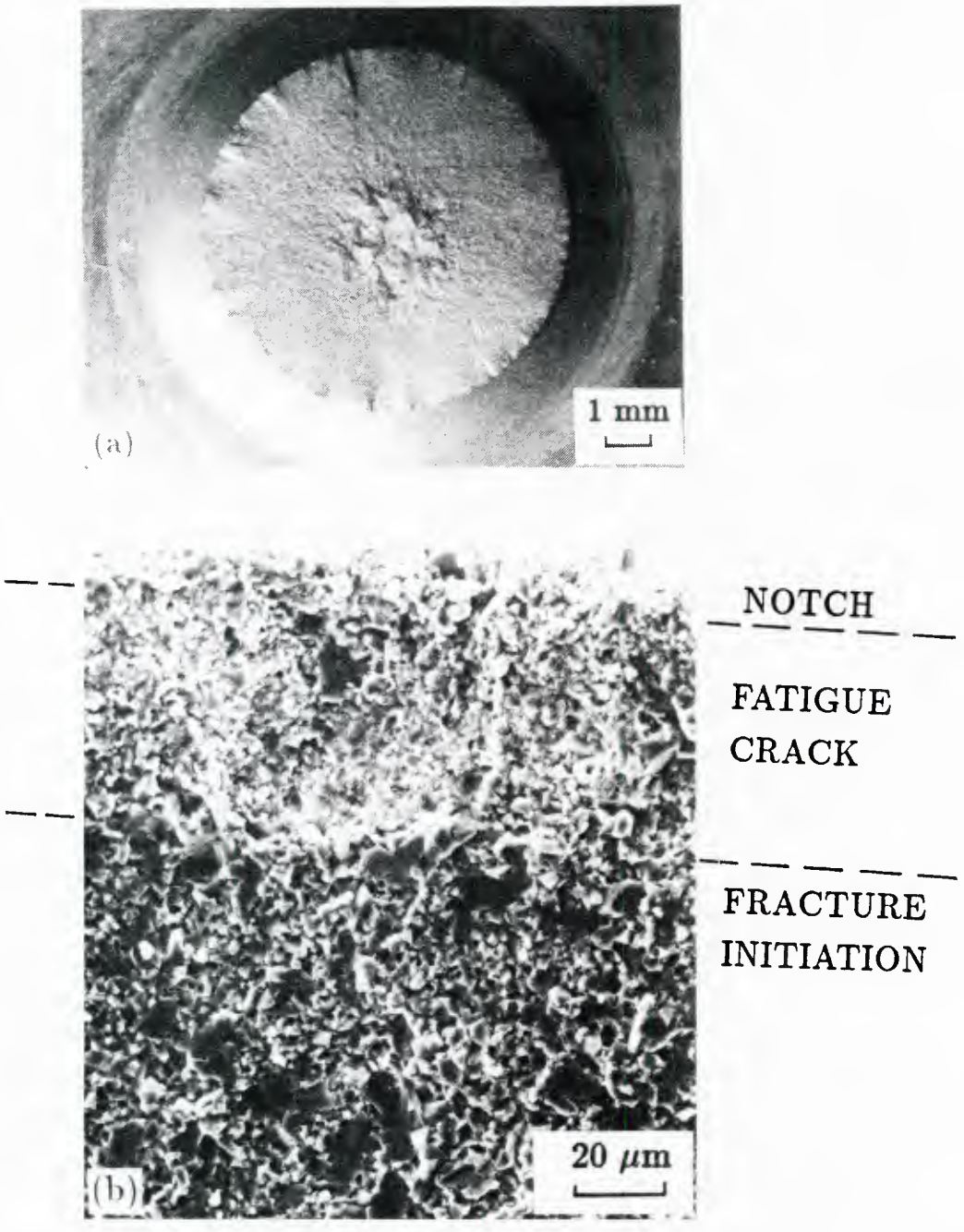

Figure 7 Photographs of dynamic Mode I fracture surfaces of polycrystalline Al_2O_3. (a) Optical micrographs (b) SEM fractograph showing the fatigue pre-crack and fracture initiation area.

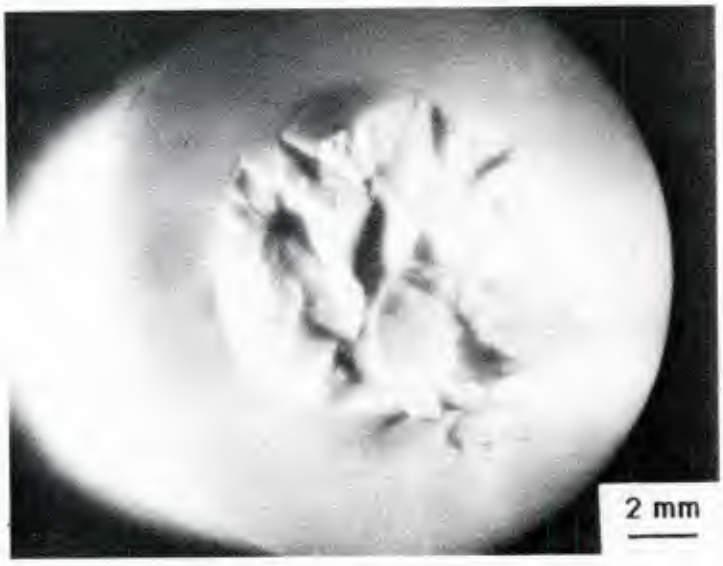

Figure 8 Optical micrograph of the quasi-static Mode III fracture surface of polycrystalline $A\ell_2O_3$.

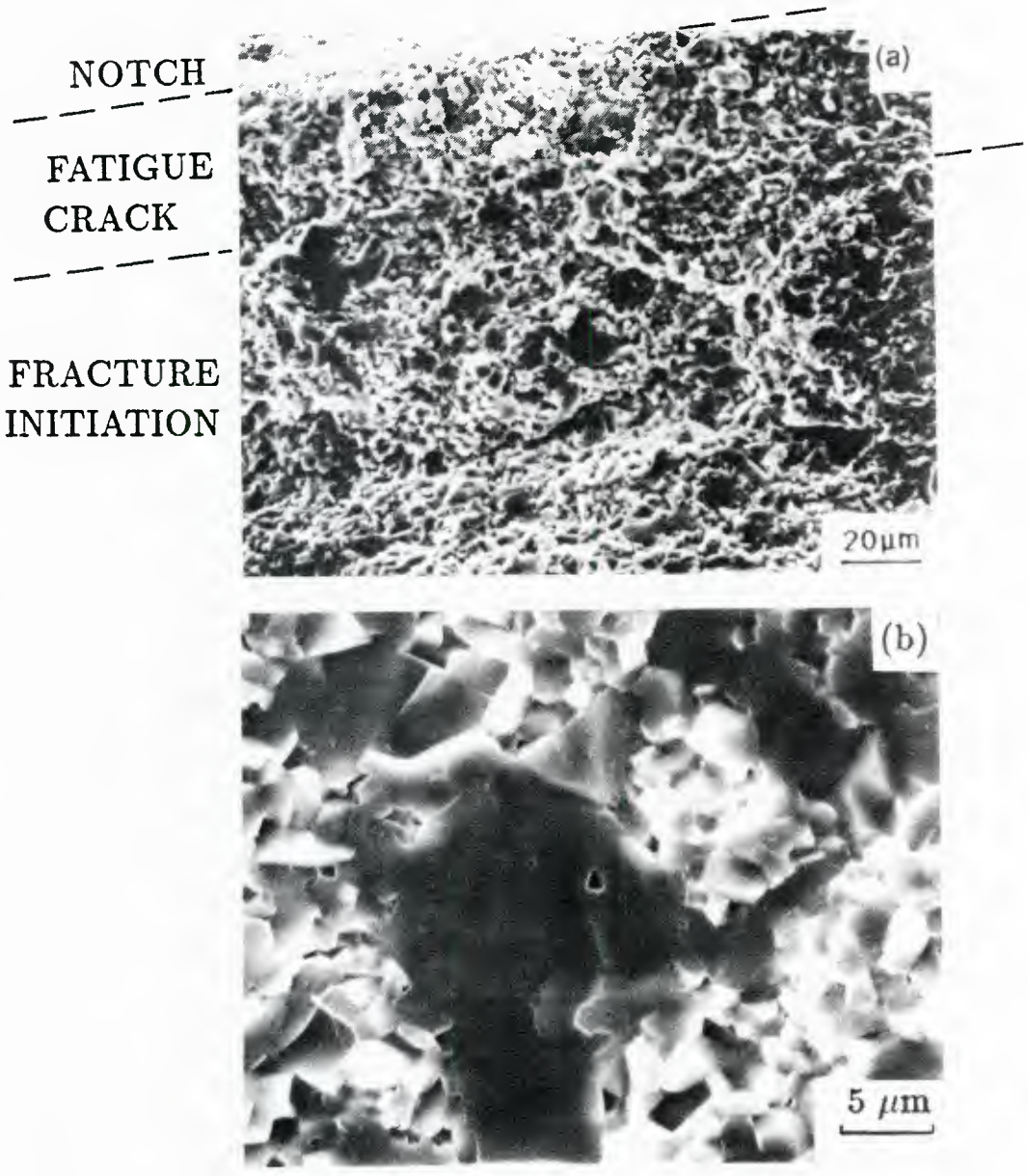

Figure 9 SEM fractographs of a quasi-static Mode III fracture surface of polycrystalline Al_2O_3. (a) shows the fatigue pre-crack and fracture initiation area, and (b) shows the transgranular facets in the fracture initiation area.

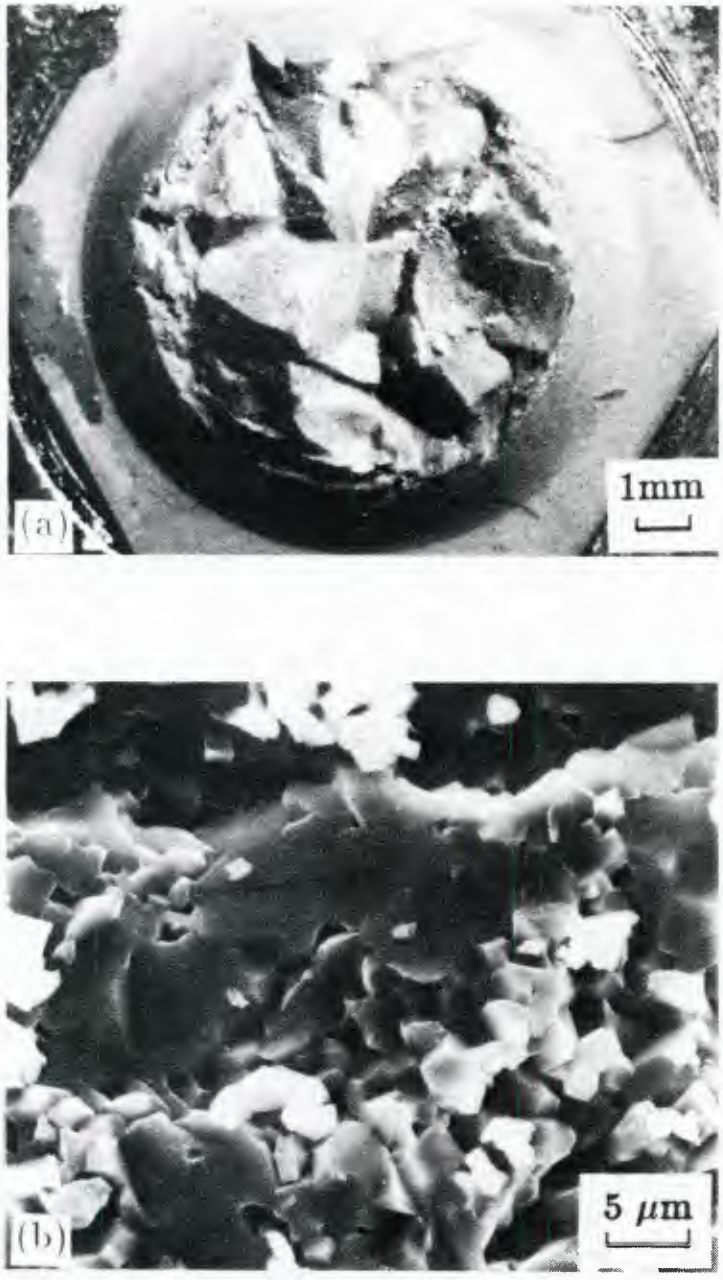

Figure 10 Dynamic Mode III fracture surface of polycrystalline Al_2O_3. (a) Optical micrograph. (b) SEM fractograph showing the transgranular facets in the fracture initiation area.